Journal of Photochemistry and Photobiology A: Chemistry 200 (2008) 114–125

Contents lists available at ScienceDirect

Journal of Photochemistry and Photobiology A: Chemistry

journal homepage: www.elsevier.com/locate/jphotochem

Fluorescence properties of (*R*)- and (*S*)-[1,1′-binaphthalene]-2,2′-diols solutions and their complexes with cyclodextrins in aqueous medium

Gema Marcelo, Raquel de Francisco, María José González-Álvarez, Francisco Mendicuti*

Departamento de Química Física, Universidad de Alcalá, 28871 Alcalá de Henares, Madrid, Spain

ARTICLE INFO

Article history:
Received 24 April 2008
Received in revised form 20 June 2008
Accepted 27 June 2008
Available online 10 July 2008

Keywords:
Cyclodextrins
Inclusion complex
Fluorescence
Molecular mechanics
[1,1′-Binaphthalene]-2,2′-diol
(1,1′-binaphthol or BINOL)

ABSTRACT

Steady-state and time-resolved fluorescence techniques were used to study (*R*)- and (*S*)-[1,1′-binaphthalene]-2,2′-diol (1,1′-binaphthol or BINOL) dilute solutions of different polarity solvents, as well as their inclusion complexes with α- and βcyclodextrins (CDs) in water. BINOLs in dilute water solutions exhibited a surprisingly high fluorescence anisotropy that was explained as being due to the formation of fairly large order π–π stacking aggregates in aqueous polar media. Stoichiometries, formation constants and the changes of enthalpy and entropy upon inclusion were also obtained by measuring the variation of the fluorescence intensity with [CD] and temperature. Results agree with the formation of 1:1 stoichiometry complexes, but the association constants are rather low and very similar for both enantiomers. Molecular mechanic calculations in the presence of water were employed to study the formation of BINOL complexes with both α- and βCDs. For the most stable structures of any of the complexes only a small portion of the guests, in agreement with thermodynamics parameters and quenching experiments, penetrates inside the CD cavities. Driving forces for 1:1 inclusion processes may be dominated by non-bonded van der Waals host:guest interactions. The low guest:host binding constants and poor enantioselectivity of α- and βCDs for BINOLS may be a consequence of the BINOL aggregation in water.

1. Introduction

The most well-known cyclodextrins (CDs) are hollow macrocyclics consisting of 6 (αCD), 7 (βCD) or 8 (γCD) α(1 → 4) joined glucopyranose units. CDs exhibit a hydrophilic external face and a hydrophobic inner cavity. They are capable of forming non-covalently bonded inclusion complexes with a variety of small and large molecules, preferentially in an aqueous medium [1–4]. Complexed guest properties may be totally different from those of either the parent guest or the CD. When the guest contains a chromophore group the change of its fluorescence properties upon complexation can provide thermodynamics (the association constant, ΔH° and ΔS°) and structural information (stoichiometry and geometry of the complex) [5–33]. Molecular modelling of the complexation process, *i.e.*, molecular mechanics (MM) [10,20,27,30,35–41] and/or molecular dynamics (MD) [35,41–48] also aids in strengthening the inclusion mechanism, the geometry of the complexes and in extending the knowledge on the driving forces involved in such processes.

Chiral [1,1-binaphthalene]-2,2-diol also named 1,1′-binaphthol or BINOL (BOH) and its derivatives, either attached to a polymer chain [49–54], forming dendritic architectures [55–58] or as a small isolated molecule [59–62], have been widely used in the asymmetric synthesis field, fluorescence and electro-optical sensors in chiral molecular recognition and in enantioselective catalysts [49–70]. In fact, we reported how the incorporation of chiral 1,1′-binaphthoxy groups into the main polyphosphazene chain yields optically active materials by the formation of a helix-type secondary structure along the polymer chain [49–52]. The efficiency of energy migration along the polymer chain is very sensitive to the presence and length of these helical sequences [52].

The fluorescence properties of BOH have been employed with particular emphasis on the effects of chirality and chiral recognition [59–62,71]. However, some controversies exist with respect to their less studied photophysical properties [71]. BOH is a chromophore molecule that emits relatively poor fluorescence. In aqueous solution, however, it exhibits surprisingly larger fluorescence anisotropy values than the ones expected for a single molecule in a fluid solvent. According to several authors [59,71] the low emission is caused by excited-state rotation of the naph-

* Corresponding author at: Departamento de Química Física, Universidad de Alcalá, Crta Madrid-Barcelona, Km 32.6, 28871 Alcalá de Henares, Madrid, Spain. Tel.: +34 91 8854672; fax: +34 91 8854763.
E-mail address: francisco.mendicuti@uah.es (F. Mendicuti).

1010-6030/$ – see front matter © 2008 Elsevier B.V. All rights reserved.
doi:10.1016/j.jphotochem.2008.06.021

thol groups along the C–C single bond or photo-induced proton dissociation. Among the main reasons for these anisotropies the proton transfer from BOH hydroxyl groups to water clusters and/or the formation of dimers or larger order aggregates are suggested. As the BOH anisotropy is still large, even in media in which proton transfer is restricted, and there is a direct dependence of the anisotropy on [BOH], some authors stated that the BOH aggregation in aqueous solutions was mainly responsible for high anisotropies [71]. The formation of homoquiral and heteroquiral dimers of BOHs in chloroform by intermolecular HB interactions and the calculation of their dimerization equilibrium constants from optical rotation and UV measurements were also reported elsewhere [72].

In this paper, several steady-state and time-resolved fluorescence techniques were employed to study the complexation of *R*- and *S*-BOHs with α- and βCDs. Stoichiometries, binding constants and the thermodynamics parameters upon complexation were obtained. The combination of fluorescence polarization, quenching, lifetime measurements and the molecular mechanics calculations permits us to interpret the changes of enthalpy and entropy upon complexation, which are related to the geometry and the driving forces responsible for the formation of such complexes. In addition, a complete study of the fluorescent behavior of the free (*R*)- and (*S*)-BOHs in different solvents was performed in order to try to shed more light on the origin of the high fluorescence anisotropy values in aqueous solvents.

2. Samples and methods

2.1. Materials

The *R*- and *S*-BOH guests, depicted in Fig. 1, were purchased from Aldrich and they were used as received. The α- and βCD (Aldrich) were also used without further purifications (Fig. 1). Water content of ~10% and ~6% for the α- and βCD, respectively were obtained by TGA. Solvents employed were *n*-alcohols $H(CH_2)_nOH$, from $n = 1–7$ (Aldrich spectrophotometric grade or purity >98%) and deionized water (Milli-Q). BOH/CD solutions were prepared by weight from a double-filtered (Millipore, 0.45 μm Ø cellulose filter) aqueous BOH saturated solution. α- and βCD concentrations were in the 0–28.7, 0–16.3, 0–22.5 and 0–16.2-mM ranges for *R*-BOH/αCD, *R*-BOH/βCD, *S*-BOH/αCD and *S*-BOH/βCD systems, respectively. [BOH] was kept constant in all experiments (<10^{-6} M). Totally transparent solutions were stirred for about 2 days before measuring. Additional experiments required filtering BOH dilute solutions with different hydrophilic pore diameter size filters (Millipore, 0.1 μm Ø Durapore PVDF, 0.22 and 0.025 μm Ø cellulose).

2.2. Apparatus

Steady-state fluorescence and time-resolved measurements were performed by using SLM 8100 AMINCO and a TCSPC FL900 Edinburgh Instruments spectrofluorimeters. Characteristics and measurement conditions were described previously [22]. Due to the low fluorescence intensity the thyratron-gated lamp was substituted for a pulsed nanoled (HORIBA Jobin Ybon) which emits at 295 nm. Data acquisition was carried out by using 1024 channels with a time window width in the 50–200 ns range (depending on the lifetime of the system) with a total of 10,000 counts at the maximum. Most of the measurements were performed in the 5–45 °C temperature range at 10 °C intervals (Huber Ministat and Techne TE-8A). Decay intensity profiles were fitted to a sum of exponential decay functions by the iterative reconvolution method [73].

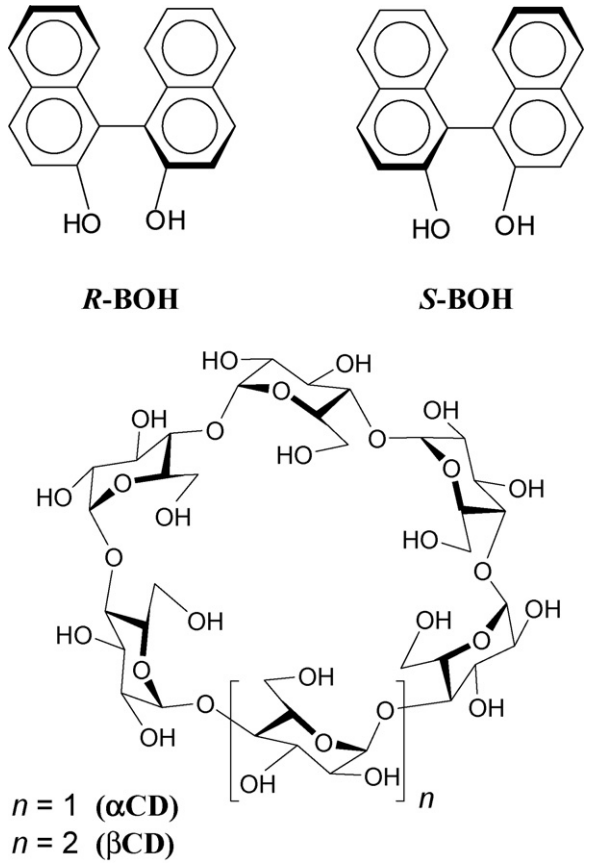

Fig. 1. Structures of *R*- and *S*-BINOLs enantiomers, α- and βCDs.

2.3. Fluorescence details

The average lifetime of a multiple-exponential decay function is defined as

$$\langle\tau\rangle = \frac{\sum_{i=1}^{n} A_i \tau_i^2}{\sum_{i=1}^{n} A_i \tau_i} \quad (1)$$

where A_i is the pre-exponential factor of the component with a lifetime τ_i of the multi-exponential function intensity decay.

From the fluorescence depolarization measurements, the anisotropy *r* is defined as [74]:

$$r = \left(\frac{I_{VV} - G I_{VH}}{I_{VV} + 2G I_{VH}} \right) \quad (2)$$

where I_{xy} is the intensity of the emission that is measured when the excitation polarizer is in position *x* (V for vertical, H for horizontal), the emission polarizer is in position *y*, and the *G* factor ($=I_{HV}/I_{HH}$) corrects for any depolarization produced by the optical system.

The dynamic quenching of a single excited species by a quencher (Q) follows the known Stern–Volmer equation [75]. Stern–Volmer plots of fluorescence intensities from steady-state measurements can give information about the quencher to chromophore accessibility.

2.4. Theoretical methods

Molecular mechanic**s** (MM) calculations were performed with Sybyl 6.9 [76] and the Tripos Force Field [77] in the presence of water. Characteristics and methods were similar to those described previously [22,26,27,34,39]. Guest charges were obtained

by MOPAC (AM1) [78]. The initial structure of both BOH enantiomers, depicted in Fig. 2, was the most stable after performing a search by changing the torsional angle along the C–C single bond between both naphthol groups, followed by optimization in vacuo ($\varepsilon = 3.5$, conjugate gradient 0.2 kcal mol^{-1} Å^{-1}). For this conformation dihedral angles between both aromatic rings are 81.7° and 83.2° for *R*-BOH and *S*-BOH, slightly smaller than the values reported from crystal structure analysis [79]. Binding host–guest energy, $E_{binding}$ (or any non-bonded energy interaction), was obtained as the difference between the potential energy of the system and the sum of the potential energies of the isolated guest and host. Strain energy is the sum of bond stretching, bond angle bending and torsion energy terms.

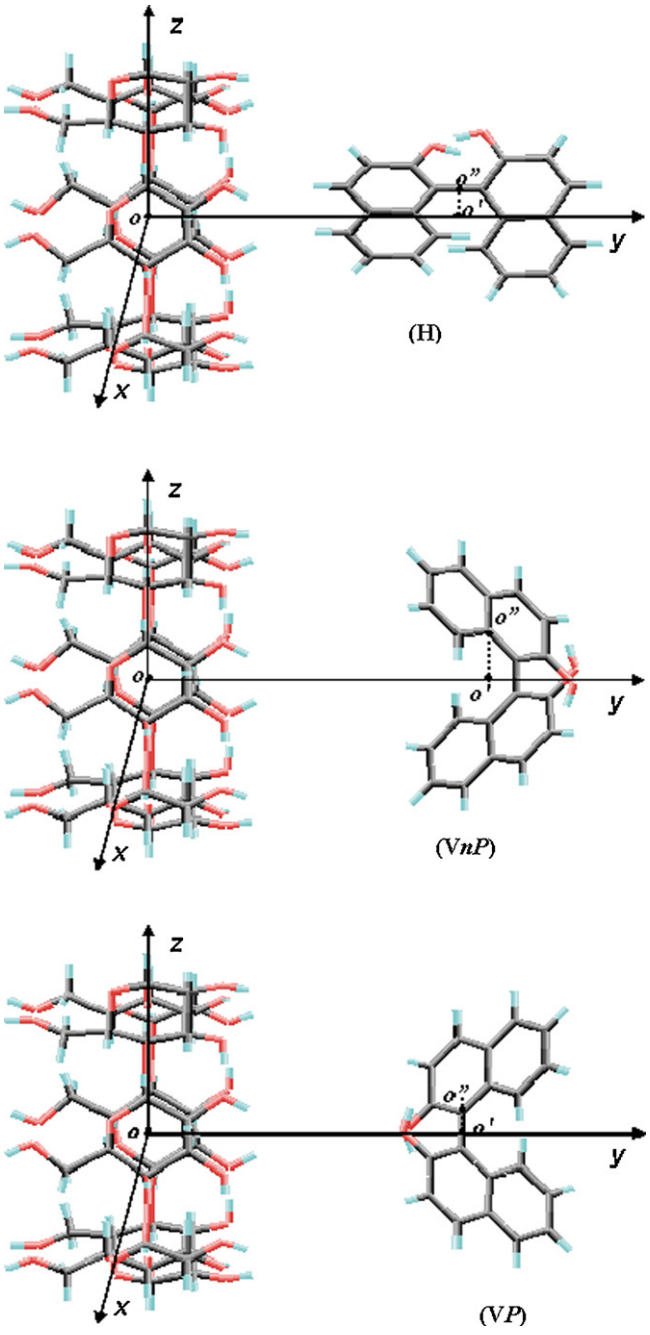

Fig. 2. Coordinate systems used to define BOH:CD complexation processes. Three orientations V*P*, Vn*P* and H for the BOH approaching to CD were considered.

Three parameters, the oo' projection on the y coordinate, the dihedral angle between the yz and the $oo'o''$ planes (θ) and the $oo'o''$ angle (δ), define the guest orientation relative to the CD host. Calculations were performed where the BOH guest approached the CD by three different orientations (depicted in Fig. 2) named H (horizontal), VnP (vertical non-polar) and VP (vertical polar). The most feasible guest–host orientations for the approaching were obtained from the critical analysis of $E_{binding}$, obtained by scanning δ, θ and y parameters in vacuo. Once the most feasible δ and θ were fixed the 1:1 complexation was simulated by approaching BOH to the CD along the y coordinate from $y = 20$ to -20 Å at 0.5 Å steps. Each generated structure generated was solvated (PBC conditions), optimized and analyzed.

3. Results and discussion

3.1. Absorption and excitation spectra

Absorption spectra for BOHs and BOH/CD solutions of both enantiomers in the 250–350 nm range exhibit main bands placed at approximately 280 and 336 nm with shoulders around 272, 292 and 325 nm. Absorption increases with the CD content for any of the systems studied. BOH excitation spectra in the absence of CD, as well as in presence of it, show bands centered at approximately 295 and 338 nm which are accompanied by a shoulder at 325 nm.

3.2. Emission spectra

Emission spectra of aerated water solutions, either for free *S*- and *R*-BOH or in the presence of CDs, upon excitation of 294 nm (some of them depicted in Fig. 3) showed two bands placed at ~355 and ~380 nm. Some characteristics of these spectra are (a) poor fluorescence intensity due to the low fluorescence quantum yield (Φ_f) of both enantiomers in water ($\Phi_f = 0.010$ and 0.016 for *R*- and *S*-BOH in water at 25 °C); (b) an enhancement of the fluorescence intensity takes place upon addition of CD, the amount of which depends on the type of CD and temperature; higher fluorescence intensity variations with [CD] were obtained for the *R*- and *S*-BOH complexes with βCD than with αCD; and (c) the spectra neither show isosbestic points, nor exhibit any substantial fluorescence broadening to the red at any [CD] and temperature that could denote the presence of intermolecular BOH excimers.

Fig. 4 shows the increase of fluorescence intensity (area under emission spectrum) with [βCD] for the *S*-BOH/βCD system at different temperatures, as well as the intensity change for the four systems at 25 °C in a comparative way.

3.3. Lifetime measurements

Fluorescence intensity decay measurements at 355 nm upon excitation of 295 nm for isolated BOHs and BOH/CDs water solutions were performed in the 5–45 °C temperature range. Intensity profiles, either for free BOHs or in the presence of CDs, were fitted to double-exponential decays. Both BOHs exhibit a short lifetime component close to ~1.5 ns, whose contribution is in the 80–90% range, and a long one around ~10 and ~6 ns for *R*- and *S*-BOH, respectively. According to Eq. (1) these results provide average lifetimes $\langle\tau\rangle$ for *R*-BOH and *S*-BOH of ~2.4 ± 0.7 ns and ~3.4 ± 0.6 ns at 25 °C that scarcely change with temperature. In the presence of CD two components were also observed: (a) a fast lifetime component that does not differ much from the one for the isolated BOHs and whose value ranges between 1.6 and 2.1 ns; (b) a longer lived component that varies in the 9.1–10.8 ns (6.4–6.8 ns)

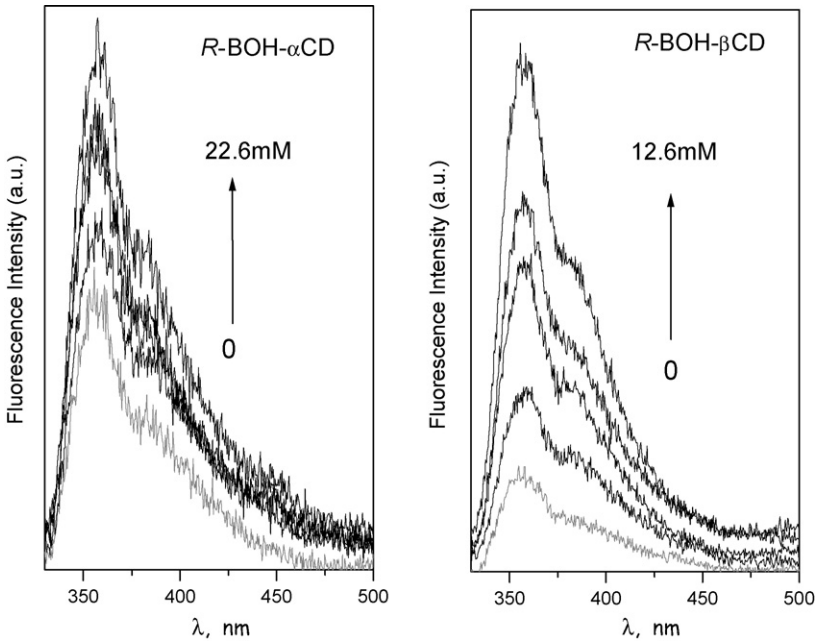

Fig. 3. Uncorrected emission spectra of *R*-BOH aerated aqueous solutions and in the presence of α- and βCDs at different [CD] at 25 °C upon λ_{exc} = 294 nm.

range for the *R*-BOH/CD (*S*-BOH/CD) system, regardless of what the CD-type was. Despite the value of the latter component, it does not mean that the *R*-BOH/CD systems exhibit larger values for ⟨τ⟩ than the *S*-BOH/CD ones. The addition of CDs simply means a little increase in ⟨τ⟩, which sometimes falls within the uncertainty measurement, for any of the systems studied. ⟨τ⟩ is not an appropriate property to study the complexation of BOHs as it was for another guest containing naphthalene chromophore [22,27,34].

3.4. Thermodynamics of complexation

For a BOH:CD_n complex whose global equilibrium can be written as

$$BOH + nCD = BOH : CD_n \quad (3)$$

the complexation constant is related to the fluorescence intensity *I* (measured as the area under emission spectrum) and $[CD]_0$ as

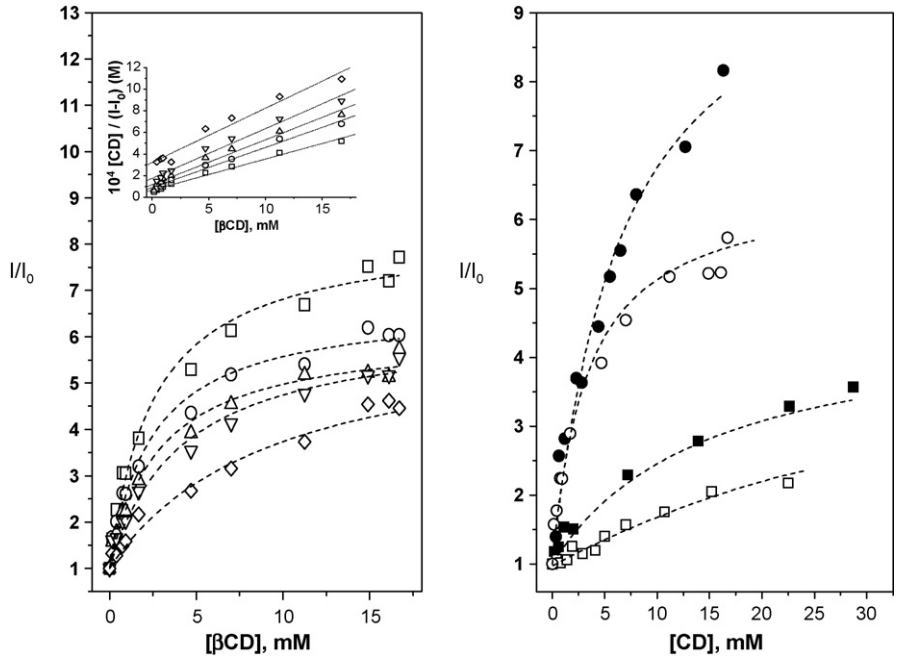

Fig. 4. (Left) Fluorescence intensities, measured as area under emission spectrum, relative to the one in the absence of CD, I/I_0 *vs.* [CD] at different temperatures: 5 °C (□); 15 °C (○); 25 °C (△); 35 °C (▽); and 45 °C (◊) for *S*-BOH/βCD system. Superimposed are the linear plots according to Eq (5). (Right) I/I_0 *vs.* [CD] for *R*-BOH (filled symbols) and *S*-BOH (open symbols) in the presence of αCD (squares) βCDs (circles) at 25 °C. Curves were obtained by adjusting the experimental data to Eq (4).

Table 1
Association constants K and $I_\infty/I_0 (= \Phi_{BOH:CD_n}/\Phi_{BOH})$ obtained from the non-linear and linear (in parentheses) adjustments for *R*-BOH and *S*-BOH in the presence of α- and βCDs at different temperatures

T (°C)	αCD		βCD	
	$\Phi_{BOH:CD_n}/\Phi_{BOH}$	K (M^{-1})	$\Phi_{BOH:CD_n}/\Phi_{BOH}$	K (M^{-1})
R-BOH				
5	5.7 ± 0.2	190 ± 38 (136 ± 15)	10.0 ± 0.4	443 ± 59 (462 ± 44)
15	5.6 ± 0.3	159 ± 38 (112 ± 18)	10.2 ± 0.6	408 ± 77 (440 ± 60)
25	5.5 ± 0.3	85 ± 19 (72 ± 8)	7.8 ± 0.5	404 ± 98 (301 ± 30)
35	5.5 ± 0.4	75 ± 20 (64 ± 15)	8.8 ± 0.8	285 ± 81 (223 ± 18)
45	5.6 ± 0.7	53 ± 20 (48 ± 17)	8.0 ± 0.9	265 ± 98 (194 ± 21)
S-BOH				
5	3.4 ± 0.4	80 ± 24 (69 ± 25)	8.3 ± 0.3	395 ± 52 (426 ± 79)
15	3.8 ± 0.5	55 ± 16 (52 ± 18)	6.7 ± 0.2	407 ± 56 (410 ± 68)
25	4.2 ± 1.0	28 ± 11 (38 ± 10)	6.1 ± 0.2	352 ± 49 (352 ± 76)
35	4.5 ± 1.3	24 ± 12 (29 ± 12)	6.2 ± 0.3	242 ± 41 (260 ± 49)
45	5.0 ± 2.0	15 ± 10 (12 ± 8)	5.7 ± 0.4	143 ± 30 (155 ± 27)

follows [10]:

$$\frac{I}{I_0} = \frac{1 + (I_\infty/I_0)K[\mathrm{CD}]_0^n}{1 + K[\mathrm{CD}]_0^n} \quad (4)$$

where $I_\infty/I_0 = \Phi_{BOH:CD_n}/\Phi_{BOH}$. Φ_{BOH} and $\Phi_{BOH:CD_n}$ are the fluorescence quantum yields for the free and complexed guests respectively at the excitation wavelength (in the absence of CD and at $[\mathrm{CD}] \to \infty$). Eq (4) can be reorganized as

$$\frac{[CD]_0^n}{(I - I_0)} = \frac{1}{K(I_0 - I_\infty)} + \frac{[CD]_0^n}{(I_0 - I_\infty)} \quad (5)$$

Curves depicted in Fig. 4 come from a non-linear regression analysis [80] derived from Eq (4). Table 1 collects the complexation constants obtained from these adjustments and the linear analysis from Eq (5) (also superimposed in Fig. 4) and $\Phi_{BOH:CD_n}/\Phi_{BOH}$. Adjustments correspond to 1:1 stoichiometries for all the complexes studied. As expected, quantum yields for the complexed guests are much larger than for the uncomplexed ones ($\Phi_{BOH:CD_n} > \Phi_{BOH}$) for all the systems at any temperature. The ratio $\Phi_{BOH:CD_n}/\Phi_{BOH}$ decreases with temperature but is only noticeable for BOH/βCD complexes. Moreover, $\Phi_{\Phi_{BOH:\beta CD_n}} > \Phi_{\Phi_{BOH:\alpha CD_n}}$ may be related with a better penetration and/or fit, due to the cavity size, of both BOHs when forming the complex with βCD. The average of association constants at 25 °C was approximately 80 and 33 M^{-1} for *R*- and *S*-BOH with αCD and 350 M^{-1} for any of the BOHs with βCD. This means that at [CD] = 15 mM, the fractions of *R*- and *S*-BOH complexed with αCD were 0.54 and 0.38, respectively. These fractions increase up to 0.84 when *R*- and *S*-BOH complexes with βCD. In agreement with our values, some authors [59] reported association constants for 1:1 complexes of *R*- and *S*-BOH with βCDs of 230 and 280 M^{-1}, respectively at 25 °C, concluding that βCD is not a good host for enantioselective complexation with BOHs. These association constants were relatively low compared to the values reported for the complexation of 1- and 2-naphthols with CDs. Both naphthols form 1:1 stoichiometry complexes with βCDs at 25 °C with association constants of 1230 M^{-1} [81,82] for 1-naphthol/βCD. Values of 501 M^{-1} [83] and 590 M^{-1} [84] for 2-naphthol/βCD complex were reported. 2-Naphthol, however, gives a 1:2 complex with αCD with a global constant of approximately 8750 M^{-2} [84].

The linear van't Hoff plots depicted in Fig. 5 were obtained from the average of the association constants collected in Table 1. These representations were linear taking into account the experimental uncertainties in *K*. Nevertheless, the small down-hill curvature of some of the representations would agree with $\Delta C_p^\circ < 0$, typical for the transfer of apolar molecules from water to a hydrophobic environment such as CDs [26].

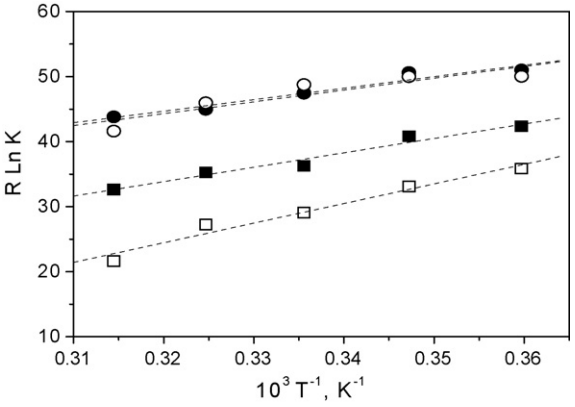

Fig. 5. Van't Hoff plots of RLn K *vs.* T^{-1} for the formation of *R*-BOH (filled symbols) and *S*-BOH (open symbols) complexes with αCD (squares) and βCD (circles) from the association constants collected in Table 1.

As showed in Table 2, BOH complexations with α- and βCDs are accompanied by $\Delta H^\circ < 0$. Negative enthalpy changes increase as the cavity size decreases. These results agree with the possibility that van der Waals (vdW) and/or hydrogen bonding (HB) attractive interactions are mainly responsible for the formation of BOH/CD complexes. These interactions, which are typically characterized by negative enthalpy changes upon complexation, should decrease, as should the absolute value of the enthalpy change, with cavity size.

The signs of entropy changes are all negative. The ΔS° value and sign upon complexation is mainly attributed to the balance of two opposite effects: the change in the ordering of the solvent shell surrounding the BOH guest or included inside the CD host, and the variation in the rotational and translational degrees of freedom of the BOH due to its association with CD. The former makes entropy increase and the latter makes it decrease. For a guest that penetrates only slightly inside the cavity or one that penetrates a little more deeply and fits tightly into it, complexation is usually accompanied by an unfavorable $\Delta S^\circ < 0$. In contrast, guests that penetrate totally but that exhibit a certain freedom of movement inside it due to the

Table 2
Thermodynamics parameters obtained from the binding constants collected in Table 1 at different temperatures

Complex	ΔH° (kJ mol^{-1})	ΔS° (J K^{-1} mol^{-1})
R-BOH/αCD	−22.1 ± 2.4	−37 ± 8
R-BOH/βCD	−17.7 ± 2.3	−12 ± 8
S-BOH/αCD	−30.1 ± 3.1	−72 ± 10
S-BOH/βCD	− 18.1 ± 4.8	−14 ± 13

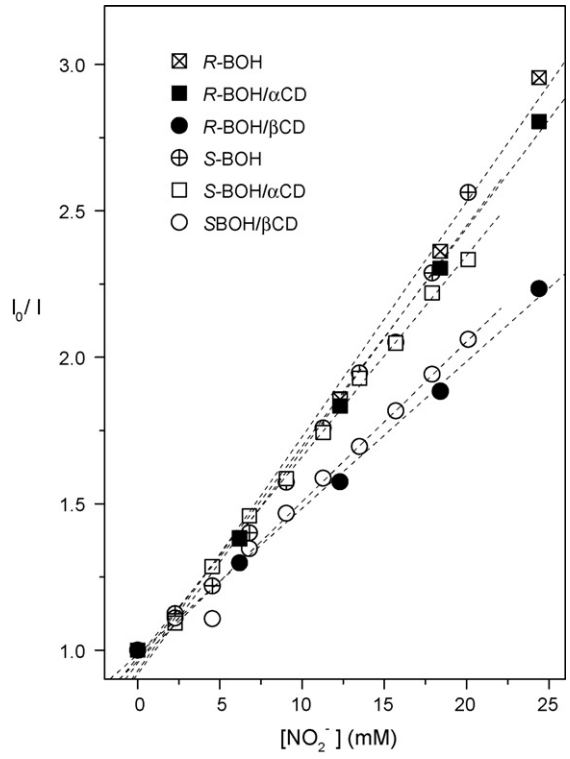

Fig. 6. Linear Stern–Volmer plots for BOH and BOH/CD water solutions at 25 °C obtained from steady-state measurements at 25 °C (correlation coefficient ≈0.994–0.999). *I* was measured as the area under the emission spectra.

relatively larger cavity size, show a $\Delta S^\circ > 0$. Several examples of this behavior on the complexation of esters derived from naphthalene carboxylic acids when complexing with CDs were reported by us [10,12,20,21,25–27,34].

The results for all BOH/CDs reveal that BOHs may not penetrate totally inside the α- and βCD cavities or that if they do their bulky character impedes any movement inside the CDs. Nevertheless, the quantitative ΔS° values may point towards a relatively better inclusion of both isomers when forming the complex with βCDs.

3.5. Fluorescence quenching

Quenching by $NaNO_2$ was carried out on BOH and BOH/CD water solutions at 25 °C. Measurements in the presence of CDs were performed at [CD] for which the fractions of complexed BOHs were similar (~0.60). Stern–Volmer $I_{[Q]=0}/I$ plots depicted in Fig. 6 were linear in the range of concentrations used. Results show that Stern–Volmer constants (K_{SV}) are larger for free BOH (~76 and ~80 M^{-1} for *R*- and *S*-BOH, respectively) than for complexed ones.

Nevertheless, K_{SV} values for the complexes of BOHs with αCD, whereas somewhat smaller, do not differ much from the values of the free BOHs (~74 and ~67 M^{-1} for *R*- and *S*-BOH/αCD, respectively). When BOH complex with βCD the values of K_{SV} (~50 and ~55 M^{-1} for *R*- and *S*-BOH/βCD, respectively), however, are smaller. These results agree with the fact that the access of the quencher to the free BOHs is quite similar to when they are complexed with αCD. This access, however, is slightly more difficult when they complex with βCDs. This may indicate that BOHs hardly penetrate inside the αCD cavity whereas they do so a little more in the βCD one. Results may agree with the rather small values for the association constants and the large negative entropy changes obtained for the complexes with αCD, as compared to the ones for the complexes with βCDs.

3.6. Fluorescence depolarization

Fluorescence anisotropies (r) were obtained from fluorescence depolarization measurements by using the L-format [74] at 355 nm upon excitation at 295 nm. Fig. 7 shows the change in r with [βCD] for the *S*-BOH/βCD system at several temperatures and the variation of r with [CD] for all systems at 25 °C. From the left panel of Fig. 7, excluding the values at the smallest CD concentrations, an increase of r with [CD] is evident for *S*-BOH/βCD (this also occurs for the *S*-BOH/βCD system). This increase, however, is not observed for the systems that contain αCDs. The increase with [CD] is associated to the increase of the fraction of the complexed form with a smaller rotational diffusion rate than for the free BOHs. More r variation with [CD] for BOH/βCD systems is a consequence of the larger binding constants for BOH:βCD complexes. r also seems to decrease with temperature at each particular CD concentration for BOH/βCD systems. This decreasing is therefore due to the increase in the rotational diffusion rate of both free and complexed forms as a consequence of the decreasing in medium viscosity.

Under the assumption that the total anisotropy is the sum of contributions due to uncomplexed and complexed guests, the following equation can be derived:

$$r = \frac{r_0 + r_\infty K\Phi[\mathrm{CD}]_0}{1 + K\Phi[\mathrm{CD}]_0} \quad (6)$$

which contains another Φ parameter that is related with the quantum yield of the complexed form and whose value depends on the excitation and emission wavelength selected.

Curves depicted in Fig. 7 for BOH/βCD systems are the results of the adjustments to Eq (6), which seem to reasonably fit the experimental anisotropy data, by using K values from steady state but removing some of the points obtained at the lowest [CD]. For BOH/αCDs these adjustments are not possible due to the low association constants. Values of r_∞ at 25 °C obtained from the adjustments to Eq (6), which may provide the anisotropies for complexed BOHs, are quite similar for both complexes with βCDs (0.193 ± 0.005 and 0.190 ± 0.011 for *R*- and *S*-BOH/βCDs, respectively).

Nevertheless, one of the main characteristics for both BINOLs is the high anisotropy values that their aqueous solutions exhibit, even in the absence of CDs.

3.7. Fluorescence of isolated BINOLs

Steady-state and fluorescence decay measurements for *R*- and *S*-BOH dilute solutions of different solvents were performed at 25 °C. The solvents, covering wide polarity (ε) and viscosity (η) ranges, were methanol/water, ethanol/water mixtures (vol%) and a series of *n*-alcohols (from methanol through 1-heptanol). Emission spectra were analogous to the ones obtained for *R*- and *S*-BOH/water solutions, and very similar for both isomers, showing two typical bands. As in water, decay profiles were bi-exponentials, exhibiting the two characteristics, whereas slightly faster than in water, lifetime components: a short one, whose contribution was always larger than 90%, and a long one which hardly contributed to $\langle\tau\rangle$ in some solvents. This latter contribution always decreased as the water content in the solvent mixtures decreased.

Fig. 8 depicts the dependence of fluorescence quantum yields (Φ_f), lifetime averages ($\langle\tau\rangle$) and fluorescence anisotropies (r) on medium polarity and viscosity for *R*-BOH. Results for *S*-BOH, not shown, are rather similar. Fluorescence quantum yields seem to be sensitive to both polarity and microviscosity surrounding BOHs. Φ_f decreases with ε and, as expected, especially when looking at the *n*-alcohol series, it increases with η. This is obviously the reason for the fluorescence increases that BOHs experience upon CD

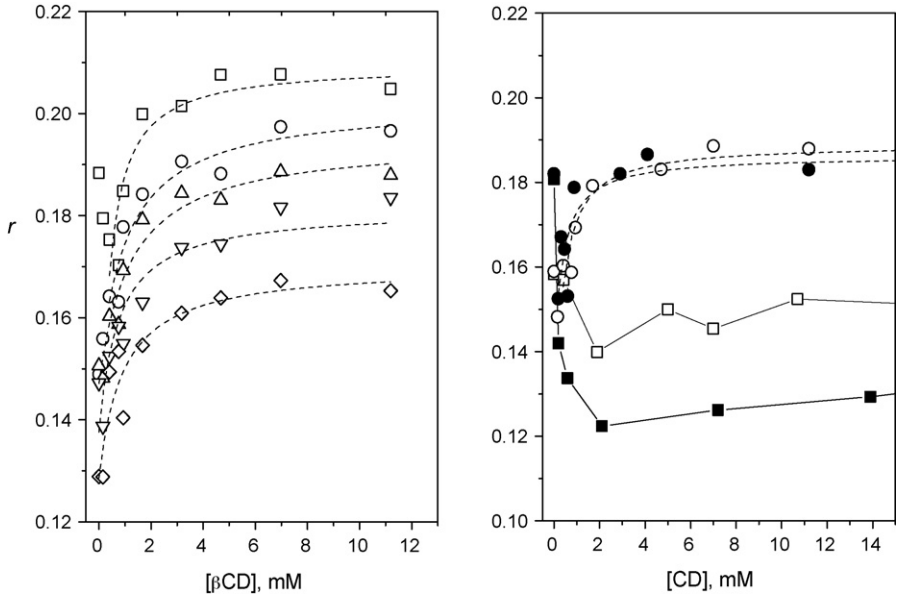

Fig. 7. (Left) Variation of the fluorescence anisotropy, r with [βCD] (λ_{em} = 355 nm, λ_{ex} = 295 nm) at 5 °C (□), 15 °C (○), 25 °C (△), 35 °C (▽) and 45 °C (◊); (right) Variation of r with [CD] for *R*-BOH/αCD (■), *R*-BOH/βCD (●), *S*-BOH/αCD (□) and *S*-BOH/βCD (○) systems at 25 °C.

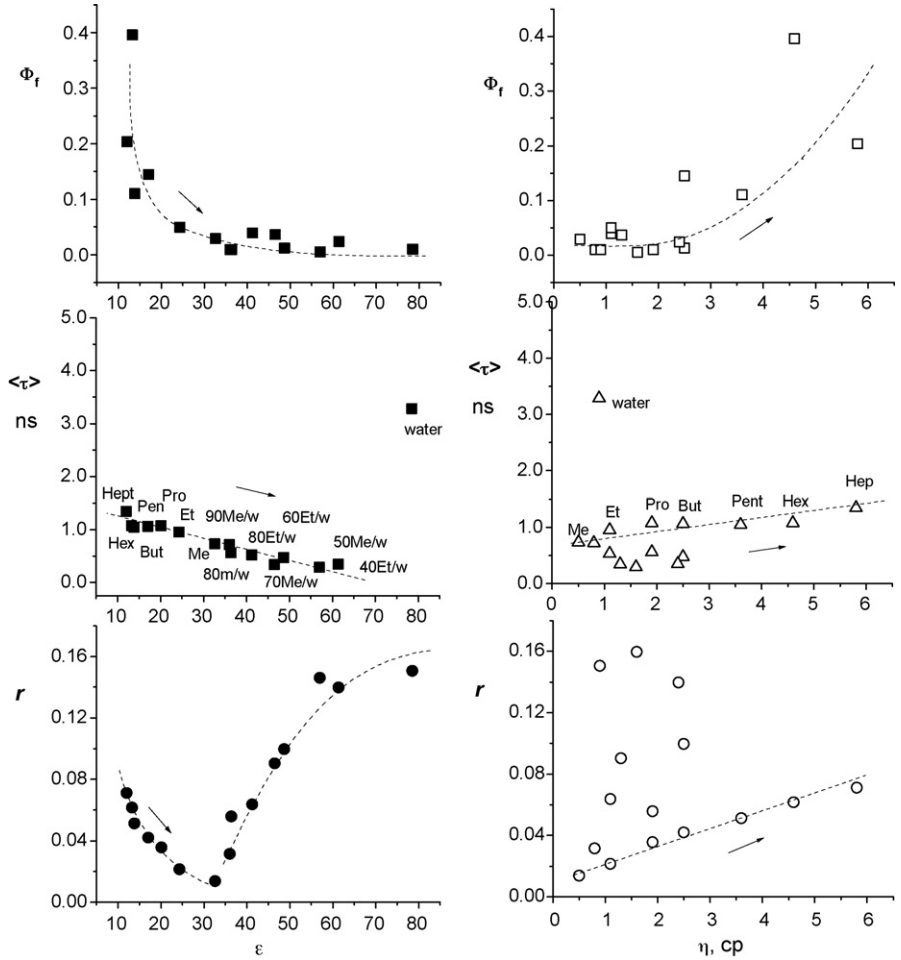

Fig. 8. Changes in fluorescence quantum yields (Φ_f), lifetime averages ($\langle\tau\rangle$) and anisotropies (r) with polarity (ε) and viscosity (η, cp) for *R*-BOH dilute solutions at 25 °C in different solvents. Solvents are methanol/water (M/W) and ethanol/water (E/W) mixtures (% v/v) and the *n*-alcohol series from methanol through 1-heptanol (Hep).

addition, as complexation implies polarity decreasing and microviscosity increasing. As Fig. 8 shows, $\langle\tau\rangle$ increases with medium viscosity but decreases with polarity. $\langle\tau\rangle$ changes, however, are less pronounced than Φ_f. The pure solvent water deviates from this trend showing much larger $\langle\tau\rangle$ compared to those obtained in any other pure solvents or water mixtures. The addition of alcohols to water makes $\langle\tau\rangle$ to decrease significantly.

r also showed severe changes with the solvent. Considering the water mixtures, the largest *r*-values were obtained for *R*-BOH in pure water and solvents with a high water content, drastically decreasing as the content of water in the solvent mixture decreases. Some authors related this increase in *r* to the increase in the polarity of the solvent [71]. However, for *R*-BOH in *n*-alcohols, *r* increases as the polarity of the medium surrounding the guest decreases. As Fig. 8 depicts, an increase in *r* with the medium viscosity is also observed. Nevertheless, the set of points that deviate from this trend showing larger *r*-values are those measured in water-containing solvents.

As stated above, among the most feasible phenomena that could account for these high anisotropy values were the proton transfer in the excited state from hydroxyl groups to water clusters and/or the dimer or high order aggregate formation [71]. The first phenomenon was investigated in 2-naphthol and other alcohols [59,71,85] suggesting that a four-water-cluster $(H_9O_4)^+$ is the proton acceptor. The aggregation must be due to intermolecular hydrogen bonding or π–π ring stacking interactions [71].

To shed more light on the possibility of proton transfer as the cause for the anisotropy values, the pH dependence of *r* was obtained from the anisotropy emission spectra for *R*-BOH/water solutions of different pHs. These pHs were reached by using phosphate (pH = 4–8) and carbonate buffers (pH = 10) and a HCl water solution (pH = 1). Fig. 9 depicts the normalized emission spectra for *R*-BOH water dilute solutions at different pHs. They are very similar in shape for pH < 8, but the normalized intensity slightly decreases with pH at the longest wavelengths. However, the spectrum is noticeably shifted to the red at pH 9.5. This change may be attributed to the BOH deprotonation. Fig. 9 also shows the fluorescence anisotropy emission spectra for *R*-BOH at pH 1 and 9.5. Table 3 collects anisotropies for *R*-BOH/water solutions as a function of pH obtained from the anisotropy emission spectra under several experimental conditions. Results, which are reproducible, exhibit an increase in *r* as the pH decreases. If the large anisotropy values were due to a proton transfer to the water cluster the effect should be the opposite, as the effect would be diminished at the lowest pHs. The proton transfer may not be the cause of the large anisotropies observed for BOHs aqueous solutions.

Table 3
Anisotropy values for *R*-BOH/water solutions obtained from the anisotropy emission spectra at 25 °C by averaging the *r* values in a window of 10 nm around 355 nm upon the excitation of 278 nm[a] or 295 nm[b]

pH	r^a	r^b
1.0	0.0761 ± 0.039	0.1970 ± 0.0227
4.5	0.0807 ± 0.0403	0.1387 ± 0.0158
7.1	0.0034 ± 0.0211	0.1087 ± 0.0128
8.0	0.0038 ± 0.0216	0.1044 ± 0.0112
9.5	0.0027 ± 0.0454	0.0743 ± 0.0228

[a] [*R*-BOH] = 40 μM.
[b] [*R*-BOH] = 20–40 μM.

To study the presence of aggregates as the source of the anisotropy values, the fluorescence properties of *R*-BOH were investigated as a function of [*R*-BOH] using a methanol/water (50/50) mixture as solvent. Excitation spectra, not shown, exhibit two typical bands centered ∼292 and ∼336 nm. While increasing the intensity with [*R*-BOH], the shape of the spectra and ratios of both

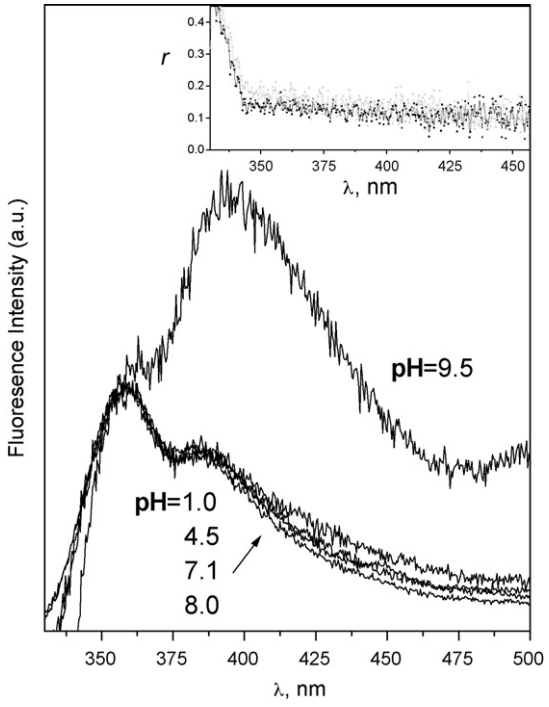

Fig. 9. Normalized (at 355 nm) emission spectra for *R*-BOH diluted water solutions at different pH and fluorescence emission anisotropy spectra upon 295 nm of excitation at pH 1.0 and 9.5 at 25 °C.

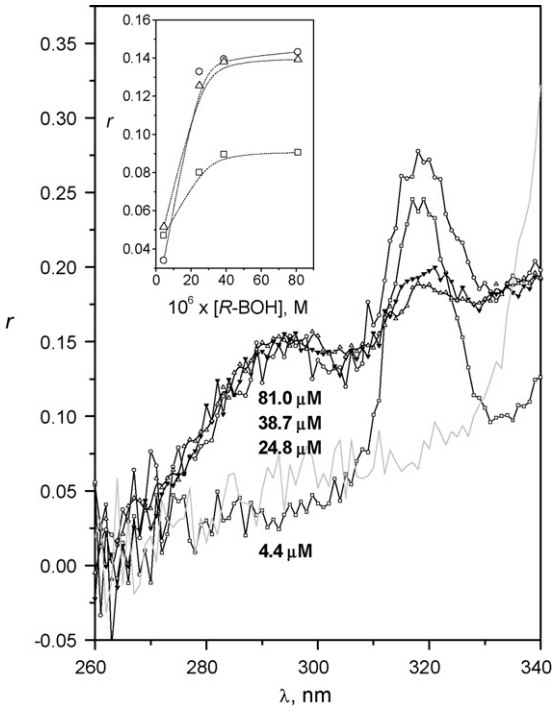

Fig. 10. Fluorescence anisotropy excitation spectra for *R*-BOH dilute water:methanol (50:50) solutions at different concentrations upon λ_{em} = 355 nm and upon 385 nm at [*R*-BOH] = 4.4 μM (gray). Superimposed is the variation of anisotropy with [*R*-BOH] obtained from the anisotropy excitation or emission spectra by a averaging the *r*-values in a window of 10 nm around: 355 nm upon λ_{exc} = 278 nm (□); 295 nm upon λ_{em} = 278 nm (○) and 295 nm upon λ_{em} = 385 nm (△).

Table 4
Anisotropy values obtained from the anisotropy emission spectra by averaging the *r* values in a window of 10 nm around 355 nm upon the excitation of 295 nm at 25 °C for different *R*-BOH solutions that were filtered with filters of several diameter pore sizes

Filter size Ø (μm)	Water[a]	Water:methanol[b]	*n*-Pentanol[c]
0.45	0.1308 ± 0.0316 (3.28)	0.1462 ± 0.0730	0.0494 ± 0.0145 (1.05)
0.22	0.0340 ± 0.0116 (2.49)	0.0488 ± 0.0029	0.0483 ± 0.0161
0.10	0.0323 ± 0.0099 (2.35)	0.0331 ± 0.0370	0.0559 ± 0.0150
0.025	0.00129 ± 0.0165 (2.16)		0.0552 ± 0.0164 (1.08)

In parentheses are some ⟨τ⟩ ns values.
[a] Saturated water solution.
[b] Water:methanol (50:50); [*R*-BOH] = 38.6 μM.
[c] Saturated-pentanol solution.

bands do not change with the concentration. Something similar occurs with the emission spectra that do not substantially differ from each other.

Fig. 10 exhibits the fluorescence anisotropy excitation spectra at several *R*-BOH concentrations. *r* slightly increases with the excitation wavelength and concentration. The band at around 320 is attributed to the Raman of the solvent that increases as the [*R*-BOH] decreases and totally disappears when the emission wavelength selected is displaced from 355 nm to the red. Superimposed is the *r* variation with [*R*-BOH], which increases with concentration. This seems to indicate the presence of BOH aggregates which are probably responsible for the large anisotropy values in the presence of water, either pure water or water mixtures. This would explain the decreasing in *r* as the water content decreases, but also the decreasing in ⟨τ⟩ as a consequence of the decrease in the contribution of the larger lifetime component and the increasing in Φ_f. This means that the larger component could be attributed to the associated BOH. These aggregates would also be favored at the lowest pHs.

The decreasing in *r* when adding small amounts of CD to BOH/water solutions (Fig. 7) may be attributed to the displacement of the aggregation equilibrium towards the un-associated BOH by formation of the 1:1 BOH/CD complex with the latter form.

Whereas the presence of BOH aggregates by inter-HB in polar aqueous solvents is quite improbable, some experiments were performed in the presence of KBr salt in order to know more about the type of aggregates. Excitation and emission spectra for a [*R*-BOH] = 81.0 μM water/methanol solution in the presence of KBr (0.5 M), do not exhibit any change in either spectra with respect to the ones obtained in its absence. Neither does the addition of salt reveal any substantial change in the *r*-values, showing that the aggregates probably do not take place via intermolecular HB, as the presence of salt would usually destroy them. Nevertheless, the formation of BOH dimers by intermolecular HB in apolar solvents such as chloroform was described elsewhere [72]. However, we believe that the increase in the anisotropy observed in Fig. 8 under $\varepsilon < 30$ must be more due to the increase in the medium viscosity than to the presence of such HB aggregates.

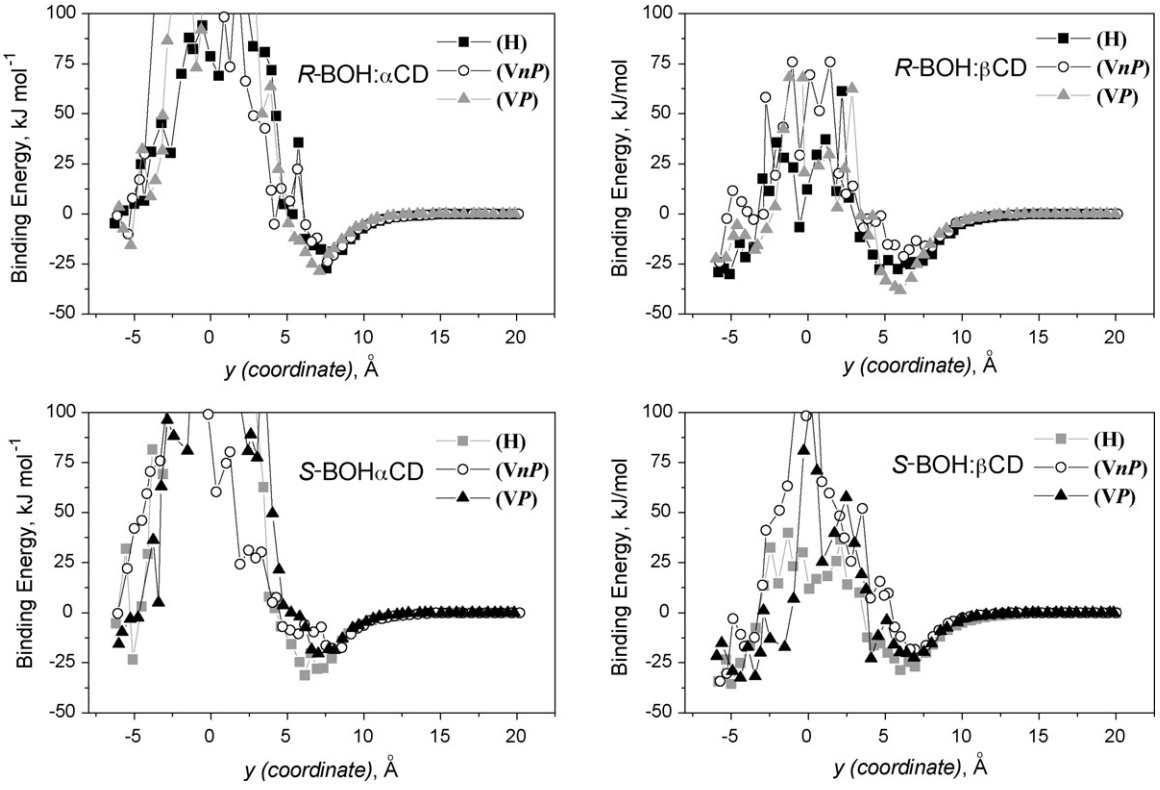

Fig. 11. Binding energies as a function of the guest-host distance (Å) along the y coordinate for the BOH complexation processes with α- and βCDs by different guest-to-host approaching.

In addition, a complete *R*-BOH/βCD complexation study in the presence of KBr (0.5 M) was also performed. Results, not shown, provide association constants and thermodynamics parameters that are similar to those in the absence of salt.

All the results, therefore, provide evidence to support the idea that the aggregate formation is driven by π–π staking in polar aqueous solvents ($\varepsilon > 35$). Decreasing medium polarity (water content) and/or increasing the pH (BOH has an acid character) in medium would mean favoring the un-aggregated form.

Totally transparent samples filtered through 0.45 μm Ø hydrophilic filters were used in all experiments. Nevertheless, to assess the order of such aggregates, fluorescence anisotropy excitation spectra were measured in several *R*-BOH solutions that were successively passed through filters with different pore sizes. Table 4 shows that the anisotropy for those solutions that contain more polar solvents (saturated *R*-BOH water or water:methanol at [*R*-BOH] = 38.6 μM solutions) monotonically decreases as the pore diameter decreases from 450 nm to 25 nm. The fluorescence intensity, as well as the values of $\langle\tau\rangle$, also monotonically decreases in the same direction. This may imply that BOHs in polar water containing solvents exhibit a wide distribution of quite large order aggregates by the interaction of hydrophobic parts. It is hardly surprising that the emission spectra from these solutions do not provide evidence on the presence of intermolecular BINOL excimers from these aggregates, as binaphthol intermolecular excimers, like biphenyl excimers, are not stable in homogeneous solutions [86]. This evidence was reported earlier by us [51]. When solvents are relatively apolar ($\varepsilon < 35$) these high order aggregates do not appear. As shown in Table 4, *R*-BOH/1-pentanol saturated solutions do not exhibit any apparent change either in the anisotropy, in the fluorescence intensity or $\langle\tau\rangle$ upon filtration.

3.8. Molecular mechanics calculations

Fig. 11 depicts changes of $E_{binding}$ for *R*- and *S*-BOHs upon approaching α- and βCDs for three H, Vn*P* and V*P* guest orientations. Nevertheless, these three orientations provide quite similar $E_{binding}$ changes. In general both BOHs, due to their relatively large size, exhibit very high repulsive barriers beginning at around $y = 5$ Å, which makes them penetrate only slightly inside the CD cavities. In fact, minima binding energies (MBE) are reached at $y = 7.1$ Å; $E_{MBE} = -28.6\ kJmol^{-1}$ ($y = 6.1$ Å; $E_{MBE} = -31.3\ kJmol^{-1}$) for the *R*-BOH (*S*-BOH) complexation with αCD. When *R*-BOH (*S*-BOH) approaches βCD the structure of MBE is achieved at $y = -6.0$ Å; $E_{MBE} = -38.3\ kJ\ mol^{-1}$ ($y = 6.0$ Å; $E_{MBE} = -28.6\ kJ\ mol^{-1}$). It is remarkable that *R*-BOH prefers to approach by the V*P* orientation whereas *S*-BOH does so preferentially by the H orientation. Both BOHs slightly penetrate into the αCD cavity and only a little more into the βCD one. Fig. 12 shows the structures of minima binding energies. The fact is that, whatever the complexes are, most of the guest molecules are exposed to the water. The breaking of the ordered water around the guest and inside the host cavities hardly contributes here to the entropy increase, the loss of freedom degrees being responsible for $\Delta S^{\circ} < 0$. These structures may corroborate the similarity in r_{∞} for both complexes with

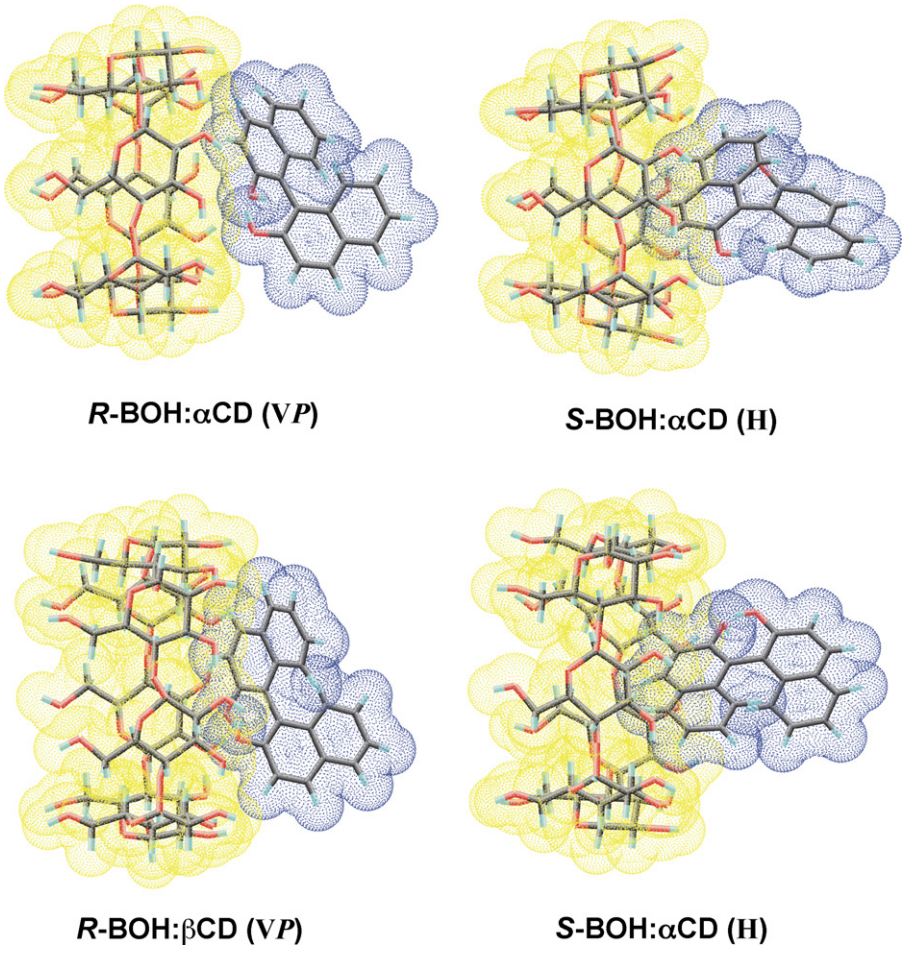

Fig. 12. Structures for the complexes that provide minima binding energies (MBE).

βCD due to the comparable structure size for both BOH/βCD complexes. They would also agree with the different behaviors observed in the quenching experiments for both BOH/αCD and BOH/βCD systems.

More than 90% of the $E_{binding}$ at the MBE is always due to non-bonded van der Waals interactions. Electrostatics represents a minor contribution to the total binding energy. Nevertheless, this contribution is always favorable and even more so at the *y*-coordinate corresponding to the energy barrier.

4. Conclusions

BINOLs form complexes of 1:1 stoichiometry with α- and βCDs. The stability constants for the complexes with βCD are somewhat larger than those for complexes formed with αCDs. Similar association constants for the complexation of both enantiomers were obtained. BINOL complexations with α- and βHPCDs are accompanied by negative values for ΔH° and ΔS°. In agreement with the fact that vdW and/or HB attractive interactions are the driving forces for the formation of BOH:CD complexes, the absolute ΔH° values decreases as the cavity size increases.

ΔS° values indicate that both BINOLs hardly penetrate inside the CD cavities, although they do so a little more when complexed with βCD. The latter statement agrees with quenching experiments and does not disagree with r_{∞} values. MM calculations also showed that 1:1 complexes of BINOLs with CDs are feasible to form and that the non-bonded van der Waals interactions are mainly responsible for complex stability. BINOLs hardly penetrate inside the αCD cavity and only a little more inside the αCD one. BINOLs in water containing solutions exhibit unexpectedly large fluorescence anisotropy values. Experimental evidence strongly pointed to the formation of high order π–π stacking BINOL aggregates as the cause of such anisotropy values. The relatively low complexation constants and the poor enantioselectivity of CDs for BINOLs in aqueous media may be a consequence of its aggregation.

Acknowledgements

This research was supported by the Comunidad de Madrid (CAM project: S-055/MAT/0227), CICYT (project CTQ2005-04710/BQU), Ministerio de Educación (FPU grant to G.M.) and Consejería de Educación y Ciencia de la Junta de Castilla-La Mancha (grant to M.J.G-A). We wish to express our thanks to M.L. Heijnen for assistance with the preparation of the manuscript.

References

[1] J. Szejtli, T. Osa, Comprehensive Supramolecular Chemistry, vol. 3, Cyclodextrins, Elsevier, Oxford, 1996.
[2] V.T. D'Souza, K.B. Lipkowitz, Chem. Rev. 98 (5) (1998) 1741–2076.
[3] A. Harada, Acc. Chem. Res. 34 (2001) 456–464.
[4] S.A. Nepogodiev, J.F. Stoddart, Chem. Rev. 98 (5) (1998) 1959–1976.
[5] L. Flamigni, J. Phys. Chem. 97 (38) (1993) 9566–9572.
[6] E.K. Fraiji Jr., T.R. Cregan, T.C. Werner, Appl. Spectrosc. 48 (1) (1994) 79–84.
[7] A. Nakamura, S. Sato, K. Hamasaki, A. Ueno, F. Toda, J. Phys. Chem. 99 (27) (1995) 10959–110959.
[8] J. van Stam, S. De Feyter, F.C. De Schryver, C.H. Evans, J. Phys. Chem. 100 (51) (1996) 19959–19966.
[9] S. Hamai, J. Phys. Chem. B 101 (9) (1997) 1707–1712.
[10] J.M. Madrid, M. Villafruela, R. Serrano, F. Mendicuti, J. Phys. Chem. B 103 (23) (1999) 4847–4853.
[11] N. Sadlej-Sosnowska, A. Siemiarczuk, J. Photochem. Photobiol. A: Chem. 138 (2001) 35–40.
[12] A. Di Marino, F. Mendicuti, Appl. Spectrosc. 58 (7) (2004) 823–830.
[13] M. Shannigrahi, S. Bagchi, Chem. Phys. Lett. 403 (2005) 55–61.
[14] N.J. Turro, T. Okubo, G.C. Weed, Photochem. Photobiol. 35 (3) (1982) 325–329.
[15] K. Kano, I. Takenoshita, T. Ogawa, Chem. Lett. Chem. Soc. Jpn. 3 (1982) 321–324.
[16] S. Hamai, J. Phys. Chem. 93 (17) (1989) 6527–6529.
[17] G. Pistolis, Chem. Phys. Lett. 304 (1999) 371–377.
[18] P.R. Sainz-Rozas, J.R. Isasi, G. González-Gaitano, J. Photochem. Photobiol. A: Chem. 173 (3) (2005) 319–327.
[19] G.C. Catena, F.V. Bright, Anal. Chem. 61 (8) (1989) 905–909.
[20] J.M. Madrid, F. Mendicuti, W.L. Mattice, J. Phys. Chem. B 102 (11) (1998) 2037–2044.
[21] A. Di Marino, F. Mendicuti, Appl. Spectrosc. 56 (12) (2002) 1579–1587.
[22] I. Pastor, A. Di Marino, F. Mendicuti, J. Phys. Chem. B 106 (8) (2002) 1995–2003.
[23] A. Muñoz de la Peña, T.T. Ndou, J.B. Zung, I.M. Warner, J. Phys. Chem. 95 (8) (1991) 3330–3334.
[24] A.Y. Will, A. Muñoz de la Peña, T.T. Ndou, I.M. Warner, Appl. Spectrosc. 47 (3) (1993) 277–282.
[25] J.M. Madrid, F. Mendicuti, Appl. Spectrosc. 51 (11) (1997) 1621–1627.
[26] M. Cervero, A. Di Marino, F. Mendicuti, J. Phys. Chem. B 104 (7) (2000) 1572–1580.
[27] I. Pastor, A. Di Marino, F. Mendicuti, J. Photochem. Photobiol. A: Chem. 173 (3) (2005) 238–247.
[28] G. Nelson, G. Patonay, I.M. Warner, Appl. Spectrosc. 41 (7) (1987) 1235–1238.
[29] J.A.B. Ferreira, S.M.B. Costa, J. Photochem, Photobiol. A: Chem. 173 (3) (2005) 309–318.
[30] L. Serna, A. Di Marino, F. Mendicuti, Spectrochim. Acta A: Mol. Biomol. Spectrosc. 61 (8) (2005) 1945–1954.
[31] M.A. Hossain, H. Mihara, A. Ueno, Bioorg. Med. Chem. Lett. 13 (24) (2003) 4305–4308.
[32] J.W. Park, S.Y. Lee, S.M. Kim, J. Photochem. Photobiol. A: Chem. 173 (3) (2005) 271–278.
[33] S. Nigam, G. Durocher, J. Photochem. Photobiol. A: Chem. 103 (1997) 143–152.
[34] C. Alvariza, R. Usero, F. Mendicuti, Spectrochem. Acta A 67 (2) (2007) 420–429.
[35] K.B. Lipkowitz, Chem. Rev. 98 (5) (1998) 1829–1873.
[36] B.S. Jursic, Z. Zdravkovski, A.D. French, J. Mol. Struct. (Theochem.) 366 (1996) 113–117.
[37] D. Salvatierra, C. Jaime, A. Virgili, F. Sanchez-Ferrando, J. Org. Chem. 61 (26) (1996) 9578–9581.
[38] J.M. Madrid, J. Pozuelo, F. Mendicuti, W.L. Mattice, J. Colloid Interf. Sci. 193 (1) (1997) 112–120.
[39] J. Pozuelo, A. Nakamura, F. Mendicuti, J. Incl. Phenom. Macrocycl. Chem. 35 (3) (1999) 467–485.
[40] A.C.C. Lino, Y. Takahata, C. Jaime, J. Mol. Struct. (Theochem.) 594 (3) (2002) 207–213.
[41] E. Cervello, F. Mazzucchi, C. Jaime, J. Mol. Struct. (Theochem.) 530 (2000) 155–163.
[42] J. Pozuelo, F. Mendicuti, W.L. Mattice, Macromolecules 30 (12) (1997) 3685–3690.
[43] K.B. Lipkowitz, G. Pearl, B. Coner, M.A. Peterson, J. Am. Chem. Soc. 119 (3) (1997) 600–610.
[44] J. Köhler, M. Hohla, R. Söllner, H.-J. Eberle, Supramol. Sci. 5 (1998) 101–116.
[45] J. Pozuelo, F. Mendicuti, W.L. Mattice, Polym. J. 30 (6) (1998) 479–484.
[46] H. Dodziuk, W. Kozminski, O. Lukin, D. Sybilska, J. Mol. Struct. (Theochem.) 525 (2000) 205–212.
[47] X. Grabuleda, P. Ivanov, C. Jaime, J. Org. Chem. 68 (4) (2003) 1539–1547.
[48] A. Di Marino, F. Mendicuti, J. Incl. Phenom. Macrocycl. Chem. 58 (2007) 295–305.
[49] G.A. Carriedo, F.J. García Alonso, P.A. González, J.L. García Alvarez, Macromolecules 31 (1998) 3189–3196.
[50] G.A. Carriedo, F.J. García Alonso, P. Gómez Elipe, J.L. García Alvarez, M.P. Tarazona, M.T. Rodríguez Laguna, E. Saiz, J.T. Vázquez, J.I. Padrón, Macromolecules 33 (2000) 3671–3679.
[51] G.A. Carriedo, J.L. García Alvarez, F.J. García Alonso, A. Presa Soto, M.P. Tarazona, F. Mendicuti, G. Marcelo, Macromolecules 37 (2004) 5437–5443.
[52] G. Marcelo, E. Saiz, F. Mendicuti, G.A. Carriedo, F.J. Garcia Alonso, J.L. Garcia Alvarez, Macromolecules 39 (2) (2006) 877–885.
[53] Y.X. Cheng, L.W. Chen, X.W. Zou, J.F. Song, Z.L. Wang, Polymer 47 (2006) 435–440.
[54] J.F. Song, Y.X. Cheng, L.W. Chen, X.W. Zhou, Z.L. Wang, Eur. Polym. J. 42 (2006) 663–669.
[55] S. Yamago, M. Furukawa, A. Azuma, J. Yoshida, Tetrahedron Lett. 39 (1998) 3783–3786.
[56] S.Q. Hu, V. Pugh, M. Sabat, L. Pu, J. Org. Chem. 64 (1999) 7528–7536.
[57] V.J. Pugh, Q.S. Hu, L. Pu, Angew. Chem., Int. Ed. 39 (2000) 3638–3641.
[58] P. Rajakumar, K. Ganesan, Tetrahedron: Asymmetry 16 (2005) 2295–2298.
[59] K. Kano, Y. Yosshiyasu, S. Hashimoto, J. Chem. Soc., Chem. Commun. (1989) 1278–1279.
[60] F.H. Billiot, M.E. McCarrol, E.J. Billiot, I.M. Warner, Electrophoresis 25 (2004) 753–757.
[61] M.E. McCarrol, F. Haddadian, I.M. Warner, J. Am. Chem. Soc. 123 (2001) 3173–3174.
[62] Y. Xu, M. McCarroll, J. Phys. Chem. A 108 (2004) 6929–6932.
[63] M.H. Xu, J. Lin, Q.S. Hu, L. Pu, J Am. Chem. Soc. 124 (2002) 14239–14246.
[64] L. Pu, Chem. Rev. 98 (1998) 2405–2494.
[65] Q.H. Fan, Y.M. Li, A.S.C. Chan, Chem. Rev. 102 (2002) 3385–3466.
[66] H.C. Zhang, L. Pu, Macromolecules 37 (2004) 2695–2702.
[67] L. Pu, Chem. Rev. 104 (2004) 1687–1716.
[68] Z.B. Li, L. Pu, Org. Lett. 6 (2004) 1065–1068.
[69] J.M. Brunel, Chem. Rev. 105 (2005) 857–898.
[70] J.M. Brunel, Chem. Rev 107 (9) (2007) 1–45.

[71] Y. Xu, M. McCarroll, J. Photochem. Photobiol. A: Chem. 178 (2006) 50–56.
[72] R. Baciocchi, G. Zenoni, M. Valentini, M. Mazzotti, M. Morbidelli, J. Phys. Chem. A 106 (2002) 10461–10469.
[73] D.V. OïConnor, W.R. Ware, J.C. André, J. Phys. Chem. 83 (1979) 1333–1343.
[74] J.R. Lakowicz, Principles of Fluorescence Spectroscopy, 2nd ed., Kluwer, New York, 1999, p. 298.
[75] J.R. Lakowicz, Principles of Fluorescence Spectroscopy, 2nd ed., Kluwer, New York, 1999, p. 242.
[76] Sybyl 6.9. Tripos Associates, St. Louis, MO, USA.
[77] M. Crark, R.C. Cramer III, N. van Opdenbosch, J. Comput. Chem. 10 (1989) 982–1012.
[78] MOPAC (AM1), included in the Sybyl package.
[79] K. Mori, Y. Masuda, S. Kashino, Acta Crystallogr. C 49 (1993) 1224–1227.
[80] MicroCal Origin 7.0, MicroCal Software Inc., Northampton, MA, USA.
[81] Q.X. Guo, X.Q. Zheng, S.H. Luo, Y.C. Liu, J. Incl. Phenom. Mol. Recogn. Chem. 26 (1996) 175–183.
[82] Q.X. Guo, X.Q. Zheng, S.H. Luo, Y.C. Liu, Chin. Chem. Lett 7 (1996) 357–360, 1996, 26, 175–183.
[83] K. Harata, Bull. Chem. Soc. Jpn. 52 (1979) 1807–1812.
[84] H.R. Park, B. Mayer, P. Wolschnn, G. Köhler, J. Phys. Chem. 98 (1994) 6158–6166.
[85] B. Valeur, Molecular Fluorescence: Principles and Applications, Wiley–VCH, Weinheim, 2002, p. 99.
[86] A.P.P. Cione, J.C. Scaiano, M.G. Neumann, F. Gessner, J. Photochem. Photobiol. 118 (1998) 205–209.